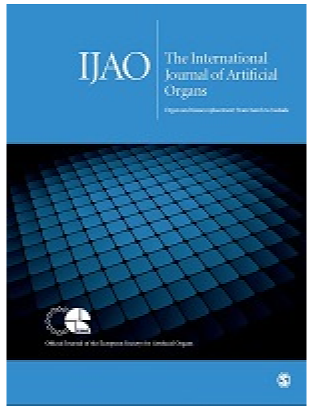

Development of a Self-Pumping Extracorporeal Blood Oxygenation Device Characterized by a Rotating Shaft with Embedded Fiber Packages

Journal:	*The International Journal of Artificial Organs*
Manuscript ID	JAO-19-0081.R3
Manuscript Type:	Original Research Article
Date Submitted by the Author:	n/a
Complete List of Authors:	Rinaudo, Antonino; Universita degli Studi di Palermo Scuola Politecnica, Engineering Pasta, Salvatore; Universita degli Studi di Palermo Scuola Politecnica, Engineering
Keywords:	Blood pump ☐ rotary < Artificial kidney, apheresis & detoxification techniques, Artificial lung < Artificial kidney, apheresis & detoxification techniques, Artificial lung design < Artificial kidney, apheresis & detoxification techniques, Artificial lung testing < Artificial kidney, apheresis & detoxification techniques, Artificial lung & respiratory support
Abstract:	Introduction: to offer respiratory support for patients with lung disease, a novel technological solution for blood pumping and oxygenation is being developed. The pump-lung system was designed to integrate fiber membranes into six packages radially embedded in a rotating hollow shaft placed along the longitudinal axis of the device. Fiber packages are inclined with respect to the rotation axis so that the rotational motion of the rotating shaft allows to obtain a self-pumping system. Method: both hemodynamic and gas transfer performances were investigated using both in-vitro experiments and in-silico flow analyses. Results: the predicted flow velocity in the pump chamber was smooth and characterized by high peripheral velocities near the housing wall. As the blood flow enters the inlet, the static pressure increased with the angular momentum imparted to the fiber packages. Experiments confirmed that the proposed pump-lung system can provide adequate blood flow and oxygen transfer over the range of intended operating conditions (0.5-5 l/min and 500-1500 rpm). Conclusions: Although the study did not include animal testing, the novel pump-oxygenator solution

	is feasible for respiratory support in patients with lung diseases.

Development of a Self-Pumping Extracorporeal Blood Oxygenation Device Characterized by a Rotating Shaft with Embedded Fiber Packages

Antonino Rinaudo[1] and Salvatore Pasta[1]

[1] Bioengineering Division, Department of Engineering, Viale delle Scienze, Ed.8, 90128, Università degli Studi di Palermo, Palermo (Italy)

* Corresponding author:
Salvatore Pasta, PhD
Professor of Industrial Bioengineering,
Department of Engineering, University of Palermo
Viale delle Science, Ed.8
90128, Palermo, Italy
Office +39 09123897277
Mobile +39 3349379694
salvatore.pasta@unipa.it

ABSTRACT

Introduction: to offer respiratory support for patients with lung disease, a novel technological solution for blood pumping and oxygenation is being developed. The pump-lung system was designed to integrate fiber membranes into six packages radially embedded in a rotating hollow shaft placed along the longitudinal axis of the device. Fiber packages are inclined with respect to the rotation axis so that the rotational motion of the rotating shaft allows to obtain a self-pumping system.

Method: both hemodynamic and gas transfer performances were investigated using both *in-vitro* experiments and *in-silico* flow analyses.

Results: the predicted flow velocity in the pump chamber was smooth and characterized by high peripheral velocities near the housing wall. As the blood flow enters the inlet, the static pressure increased with the angular momentum imparted to the fiber packages. Experiments confirmed that the proposed pump-lung system can provide adequate blood flow and oxygen transfer over the range of intended operating conditions (0.5-5 l/min and 500-1500 rpm).

Conclusions: Although the study did not include animal testing, the novel pump-oxygenator solution is feasible for respiratory support in patients with lung diseases.

Keywords: respiratory support, lung diseases, artificial lung, computational analysis

INTRODUCTION

Chronic lung disease affects 12.7 million annually and is associated with a mortality of 135,000 individuals per year [1]. Pharmacological treatment is the standard initial therapy to treat chronic lung diseases but is limited by the progression of respiratory disease and, as chronic lung disease becomes end stage, lung transplant is the only viable treatment [2]. Mechanical ventilation is conventionally available but requires invasive tracheotomy [3]. Extracorporeal gas exchange techniques, including extracorporeal membrane oxygenation (ECMO), extracorporeal and arteriovenous CO_2 removal, and intravenous oxygenation, aim to allow for a less injurious ventilatory strategy during lung recovery while maintaining near-normal arterial blood gas exchange, but preclude ambulation. Among these techniques, ECMO has demonstrated evidence to treat severe respiratory failure in pediatric patients [4]. However, the application of ECMO for adults is technical challenging as it requires an anticoagulation therapy and highly-specialized clinical team [5]. Thus, conventional ECMO can be used as a bridge to transplant but is associated with high morbidity and mortality [6]. Indeed, adverse outcomes are exacerbated by progressive deconditioning as patients are confined in ECMO. Recently, the utilization of the Maquet Cardiohelp or Quadrox along with centrifugal and the dual lumen Avalon Elite® cannula (Maquet Cardiovascular LLC, Wayne, NJ)[7, 8] simplifies ambulation and allows patients to walk, eat and exercise during therapy, thus reducing muscle deconditioning and improving patient outcomes [9]. Yet, the newer generation of ECMO systems remain bulky and cumbersome.

Lung assist devices are compact systems to supplement the respiratory function of the lung by oxygenating the blood (i.e., adding O_2) and removing carbon dioxide (i.e., removing CO_2) [10-12]. Artificial pump-lung devices belong to a class of extracorporeal carbon dioxide removal characterized by low blood flow rates. Gas exchange is accomplished by directing deoxygenated blood over a series of hollow fibers, which are permeable to O_2 and CO_2. The oxygen diffuses out of fibers and adheres to hemoglobin for systemic delivery while carbon dioxide diffuses out of the blood and into the fiber to exhaust. Several research groups have developed a number of artificial lung devices to provide either partial or full respiratory support [13-17]. The design rationale was focused on the gas exchange performance, hematologic and hemodynamic compatibility as well as the size and shape of the device. Recently, wearable systems [18] and hollow fiber oscillation techniques [19] for developing compact and lightweight artificial lungs have been proposed. Notwithstanding, the hollow fibers typically represent the largest component of an artificial lung so that the size optimization is a fundamental step in the design process of an artificial lung because compact dimensions more easily allow patients to ambulate while on support.

To optimize artificial lung size, we investigated the proof-of-concept to develop a new technological solution integrating fiber packages into a rotating hollow shaft to design an impeller-free device system. The hypothesis is that the centrifugal force induced by the rotating shaft on the blood fluid may be used to simultaneously combine blood transfer and gas exchange. This was achieved by first performing *in-silico* modeling to evaluate the pumping performance of the proposed solution, followed by *in-vitro* experiments on a prototype to quantify gas exchange. With this unique design system, we achieved over 125 ml/min oxygenation at 3.0 L/min, with a 0.27 m^2 surface area.

METHODS

Self-Pumping Device Description

The technological solution adopts a single mechanical component to simultaneously move and oxygenate blood as compared to the magnetically levitated pump-oxygenators (Figure 1). Specifically, fiber membranes are assembled in six fiber packages radially embedded in a rotating hollow shaft placed along the longitudinal device axis. Fiber packages are inclined with respect to the rotation axis (namely, the fiber package angle) so that the rotational velocity of the hollow shaft allows to obtain a self-pumping system that imposes an angular moment to the fluid and converts the kinetic energy to the pressure energy. As the shaft starts to rotate, the venous blood drawn from the patient can flow from the blood inlet to the device pump chamber. The blood passes through the hollow of the rotating shaft and then enters into the gas exchange chamber by several holes located radially with respect to the shaft axis. The gas inlet manifold is located at the top of the housing whereas the gas outlet manifold is located at the bottom of device housing. The inlet manifold distributes oxygen gas to the lumen of fibers. Since the fiber is a porous medium, the gas transfer occurs with the blood perfusing fiber packages in radial direction and the oxygen gas flowing along the longitudinal luminal direction of fibers. The oxygen diffuses across the fiber and is transferred to the blood whereas the carbon dioxide is removed. Then, the oxygenated blood is collected by a hole located in the bottom periphery of the housing to return to the patient's vasculature. The gas outlet manifold collects the gas and permits venting to the atmosphere.

Figure 2 shows the assembly of the extracorporeal device, which was designed with a cylindrical shape. The device consists of a) n.1 rotating hollow-shaft with n.6 embedded fiber packages (Oxyplus PMP 90/200, Membrana GMbH, Germany); b) n.2 sealed ball bearings (SKF 61805-2RS1, SKF®, Sweden); c) n.4 PTFE rotary lip seals for rotating shaft (Rotolip® standard, HD Slippers, Italy) and; d) n.2 custom-made polycarbonate housings. The cylindrical device had height of 200 mm and diameter of 135 mm. To form a complete pump–lung system, the device can be mounted on an electronic motor driver using an elastic joint. Table 1 summarizes technical details of the self-pumping device.

CFD-Based Analysis

The three-dimensional (3D) geometry and computational surface of the self-pumping device was generated using a computer-aided design (CAD) software package (Solidworks, v2005, Solidworks Corporation, Concord, MA, U.S.A.). Using a computational approach previously developed for cardiovascular problems [20-24], the fluid domain of the proposed device was discretized into unstructured tetrahedral elements with size of 0.1 mm using ICEM software (Ansys v.18, ANSYS, Inc.). Mesh size was obtained after analysis of the grid convergence index (GCI) to calculate the discretization error on the estimation of the shear stress. The maximum shear stress was computed for three different refinement levels, and the error was estimated for each mesh grid. For the fine mesh, the CGI between the fine and medium refinement levels was 3.5% for the maximum shear stress. The blood flow was assumed incompressible and Newtonian with a density of 1060 kg/m3 and viscosity of $3.71x10^{-3}$ Pa x s because of the relatively high shear rate of blood flow within the pulmonary artery and anastomoses. Pressure-implicit with splitting of operators (PISO) and skewness correction was used as pressure-velocity coupling algorithm to improve the convergence of transient calculations in close vicinity of distorted cells. 2^{nd} order upwind scheme was applied to discretize convective terms of momentum equations and eliminate numerical diffusion during calculations. Pressure staggering option (PRESTO) scheme as pressure interpolation method was set with 2^{nd} order accurate discretization.

Fiber packages were modeled as a porous medium since several groups highlighted that a porous medium model for fibers is acceptable. This was demonstrated comparing the results from direct modeling of individual fibers to a porous model [25] [14, 26]. However, we recognize that novel approaches to model the oxygen transfer in blood on a fiber level with CFD have been recently proposed [27, 28]. In this study, the porous medium is therefore viewed as a continuum with both solid and fluid phases in thermal equilibrium, isotropic, homogeneous, and saturated with an incompressible fluid. Hence, the porous medium has a unique porosity $\varepsilon = 0.5$ and permeability $K = 3\times10^{-9}$ m^2. To simulate different rotational shaft velocities (500, 750, 1100 and

1500 rpm), an angular velocity was applied to fiber packages with the housing assumed as a fixed wall.

A general mass transport equation for blood oxygenation based on standard convection–diffusion mass transfer equation proposed by Svitek and Federspiel [26] was implemented using user-defined subroutines (UDF) and user-defined scalars (UDS). The oxygen transfer model was coupled with continuity and momentum equations in Fluent to solve the velocity and pressure fields, gas transfer, oxygen partial pressure, and oxygen saturation. Simulations were carried out on a PC workstation with two Intel Xeon twelve-core CPUs while post-processing was done using EnSight software (v.10.2, Ansys v.18, ANSYS, Inc.).

In-vitro evaluation of hemodynamic performance

A prototype of the self-pumping oxygenator device was developed manufacturing the polycarbonate housing and the rotating hollow shaft and then included in a mock flow loop using ovine blood as a fluid. (Figure 3). The mock loop also included a heat exchanger, fluid reservoirs and deoxygenator module (Affinity, Medtronic, Minneapolis, MN) all connected by silicone tubes and plastic connectors. This set-up has led to a stable flow at inlet of the device, although experiments using two parallel loops (i.e., one for conditioning the blood and one for testing the device) should be preferable. Flow dynamic was generated by a synchronous electronic motor coupled with the rotating shaft of the device while a controller was used to change flow rates (500, 750, 1100 and 1500 rpm). For each speed setting, the blood pressure was adjusted changing the afterload resistance using clamps on silicone tubes and was continuously measured by two pressure transducers (X5072 Druck, GE Measurement & Control), which were connected to 20G catheters. Blood pressure was therefore measured at the proximal and distal ends of the device. For flow measurements, an electromagnetic flowmeter (Optiflux 5300C, Krohne, Duisburg, Germany) was placed on the plastic tube before the heat exchanger and the desoxygenator. During the test, the blood temperature was maintained at 37°C using a heat exchanger and monitored by a thermometer placed in the fluid reservoir. Hemodynamic parameters were recorded using LabVIEW software (National Instruments, Austin, TX, USA).

Experiments were performed under a gas flow to blood flow ratio of 1:1 and pure oxygen was used as sweep gas for the oxygenator under test. The sweep gas for deoxygenation through the commercial oxygenator was a N_2/CO_2 mix adjusted with a gas blender (Cole-Parmer Instrument Company, Vernon Hills, IL) in order to set the inlet condition of O_2 saturation to 65%±5%[29]. For the deoxygenation process, the mixture of N_2/CO_2 was adjusted changing the flow rate of O_2, N_2, and CO_2 in order to obtain the inlet CO_2 partial pressure of 45±2 mmHg for the test device. Once inlet conditions on O_2 and CO_2 were achieved, two samples for each flow rate were collected at inlet and outlet of the self-pumping device, respectively. Then, oxygen gas was analyzed with a blood gas analyzer (WMA-4 CO_2 Analyzer, PP System, Amesbury, MA, USA). The oxygen transfer rate was calculated based on the measured O_2 partial pressure and O_2 saturation of the blood samples at the inlet and outlet of the device. Prior to experiments, blood was collected from a slaughterhouse and then anticoagulated with anticoagulant citrate dextrose to achieve an activated clotting time greater than 500 s and filtered with 40 μm pore size filters to remove any hair or other particles. Infection was prevented by Gentamycin (0.1 g/mL). Blood properties were also adjusted to hematrocrit of 35±1%, plasma free hemoglobin of <15 mg/dL and pH of 7.4±0.1.

RESULTS

Figure 4 illustrates the velocity field as shown by streamlines for the self-pumping oxygenator device at rotational speed of 1100 rpm (flow rate of 1 l/min). Flow enters the pump chamber from the six holes located in the rotating hollow shaft because of the angular velocity of fiber packages. Streamlines reveal that the blood flow is characterized by a high peripheral circumferential velocity near the housing wall and low circulating velocity near shaft boundary. Because of the radial flow design and the shaft rotation, there is no remarkable stagnancy in the whole flow domain. The inclined fibber packages move the flow from the top to the bottom of the pump chamber so that the blood exits from the outlet and then returns to the patient.

The pressure distribution on the central cut plane of the pump chamber was obtained for the rotational speed of 1100 rpm and flow rate of 1 l/min as shown by Figure 5. Blood flow enters the inlet with low pressure (set as 0 mmHg at the inlet), and then the static pressure is gradually increased with the angular momentum imparted to fiber packages. The pressure head is developed by fiber packages and shows a magnitude at outlet of 114 mmHg. Pressure contours correlate well with the velocity field (see Figure 4). Most of the pressure loss occurs in the fiber bundle and is due to the high viscous and inertial resistances caused by fiber porosity.

Figure 6 shows the shear stress map in the pump chamber and in a cross section at mid-height of the device. We observed that the shear stress does not exceed the magnitude level of ~40 Pa at the flow rate of 1 L/min and rotational speed of 1100 rpm. High shear stress magnitudes are only seen in the region close to the fiber package periphery where the flow velocity is pronounced. In other regions, the shear stress is very low and thus unlikely to cause excessive flow-induced blood damage.

Figure 7 (A) shows the distribution of simulated oxygen transfer saturation in the middle-plane cut view of a representative fiber package. Pure oxygen is assumed in the lumen of hollow fibers while the experiment is performed under an oxygen gas flow to blood flow ratio of 1:1. When blood passes through the fiber package, it becomes gradually oxygenated upon SO_2 of 95% at distal end of fiber packages. Figure 7 (B) shows the predicted oxygen transfer rates and the experimentally-measured data at different flow rates while Figure 7 (C) displays the predicted and measured CO_2 removal. The oxygen saturation at the inlet is maintained at 65% (PO_2=40 mmHg). The oxygen transfer rate and CO_2 removal increase as the flow rate increases. Computationally predicted oxygen transfer performance and CO_2 removal are in good agreement with experimentally measured data.

Figure 7 (D) shows the hemodynamic pumping performance (H–Q curves) of the proposed device as obtained from *in-vitro* studies. These curves represent the ability of the self-pumping device to develop a pressure head against a pressure afterload at a specific flow rate and rotation speed. At 1500 rpm, the pump performance can deliver blood flow rate of 5 L/min against pressure head of 80 mmHg, approximately. When the flow rate increases, the pressure head decreases. For a fixed flow rate, a high rotational speed of the hollow shaft can generate a pronounced pressure head.

DISCUSSION

Artificial pump-lung devices, which integrate the function of pumping and oxygen transfer into one single mechanical component, are attractive as they can provide both respiratory and cardiopulmonary support [10-12]. Most of artificial lung devices adopt a magnetically levitated rotor/impeller system with a uniquely configured flow path across the fiber bundle to mitigate thromboembolic and biocompatibility problems [13, 14, 30]. The moving component is therefore a magnetically levitated rotor/impeller, which is usually supported by a mechanical shaft. Minimizing the size of artificial lungs is important to allow ambulation for patients while on support. This study aimed to provide new insights on an approach for reducing the artificial lung size as an alternative system to the impeller-based device. As a proof-of-concept, we designed a uniquely-configured pump oxygenator where packages of fiber bundles are assembled in a rotating shaft and their inclination with respect to device axis forces the blood in a circular flow path. The rotating hollow shaft with embedded fiber packages ensures that fibers are effectively and uniformly perfused to achieve maximum gas exchange efficiency. We did not observe deleterious stagnant flow or high shear stress areas because the region of slowing flow occurs at the inner shaft diameter while the housing boundary has high peripheral flow velocities. Results demonstrated the feasibility of the proposed devices by showing gas transfer efficacy and pump performances similar to those of other pump-oxygenator devices. At 3.0 L/min, we obtained 125 ml/min oxygenation with a 0.27 m^2 surface area, which is nearly 70% lower than the surface area of HLS 5.0 Cardiohelp [31]. Similarly, the compliant thoracic artificial lung (cTAL) features a pumpless device with a 2.4m^2 surface area bundle having nearly 228 ml/min oxygenation efficiency [18]. Using a surface area of 0.65 m^2, the wearable Pittsburgh Ambulatory Assist Lung system integrating a hollow fiber membrane with a centrifugal pump allows to achieve over 180 ml/min oxygenation at 3.5L/min [16, 18]. Finally, the M-lung is a device with a concentric circular blood flow path to achieve a flow of 2 L/min and oxygenation efficiency of 100 mL/min with a fiber surface area of 0.28 m^2 and priming volume of 47 mL [32]. Despite the low gas exchange area of 0.27 m^2, our prototype was developed with a high priming volume of 110 mL. This is the result of the large size of mechanical components adopted in this basic prototype to support the hollow shaft and seal the pump chamber. It is important to note that this work does not represent the characterization of a completely, self-pumping device, but rather aims to provide the preliminary analysis necessary to design one. The optimal artificial lung based on a rotating shaft with embedded fiber packages would achieve increased gas exchange efficiency and pump performance by a deep investigation of the number, size and inclination of fiber packages. Future work will be carried out for a more rigorous evaluation of the effect of the self-pumping configuration on the gas transfer, hemolysis and pump performance.

To achieve the most favorable compromise, computational flow analysis represents a valuable tool to manipulate design parameters of artificial pump-lung devices such as the saturation and pressure drop. Using a porous medium model to compute the fiber saturation, the proposed device was able to return the blood with nearly 95% of oxygen saturation with a surface area of 0.27 m^2. Using a similar computational approach, Zhang et al [14] compered the oxygen transfer of the Medtronic Affinity NT blood oxygenator with that of a mini-oxygenator. The latter demonstrated better performance with a surface area of 0.17 m^2 than the commercial oxygenator and the device here proposed. Adverse reactions can occur due to excessive fluid shear (threshold of 150 Pa) or too low fluid shear (threshold of 0.4 Pa) to determine flow-induced blood cell trauma or clotting, respectively [12, 33]. Our results evinced fluid shear magnitudes in the range of 0.6- 34.7 Pa so that cell damage should not occur in regions of high fluid shear seen at periphery of fiber packages. However, the low-flowing blood near the housing may lead to harmful flow stagnancy, potentially causing blood clotting.

CONCLUSION

Although the present study presents several limitations as the absence of blood damage tests and *in-vivo* experiments, the technological design solution for gas exchange and blood flow here proposed is attractive. Overall, results demonstrated the feasibility of integrating fiber packages into a rotating hollow shaft to simultaneously combine gas removal and blood flow and thus eliminate the impeller for moving the blood from the patient. The pump and oxygen transfer performances were evaluated by both experiments and computational flow analyses and then found similar to those of other pump-lung devices. We will continue to test the merits of our unique technological solution and believe that extensive *in-vivo* experiments and design improvements are still necessary to ascertain these data. All device components can be ideally scaled to accommodate pediatric circulatory/cardiopulmonary support. In future studies, the pump configuration will be likely improved optimizing the number of fiber packages and fiber inclination while *in-vivo* experiments will be performed to validate device feasibility for respiratory support.

REFERENCES

1. Mannino DM. COPD: epidemiology, prevalence, morbidity and mortality, and disease heterogeneity. *Chest*. 2002; 121: 121S-6S.
2. Kotloff RM and Thabut G. Lung transplantation. *American journal of respiratory and critical care medicine*. 2011; 184: 159-71.
3. Parsons PE, Eisner MD, Thompson BT, et al. Lower tidal volume ventilation and plasma cytokine markers of inflammation in patients with acute lung injury. *Critical care medicine*. 2005; 33: 1-6; discussion 230-2.
4. Jenks CL, Raman L and Dalton HJ. Pediatric Extracorporeal Membrane Oxygenation. *Critical care clinics*. 2017; 33: 825-41.
5. Zangrillo A, Landoni G, Biondi-Zoccai G, et al. A meta-analysis of complications and mortality of extracorporeal membrane oxygenation. *Crit Care Resusc*. 2013; 15: 172-8.
6. Garcia JP, Iacono A, Kon ZN and Griffith BP. Ambulatory extracorporeal membrane oxygenation: a new approach for bridge-to-lung transplantation. *The Journal of thoracic and cardiovascular surgery*. 2010; 139: e137-9.
7. Palanzo D, Qiu F, Baer L, Clark JB, Myers JL and Undar A. Evolution of the extracorporeal life support circuitry. *Artificial organs*. 2010; 34: 869-73.
8. Haneya A, Philipp A, Foltan M, et al. First experience with the new portable extracorporeal membrane oxygenation system Cardiohelp for severe respiratory failure in adults. *Perfusion*. 2012; 27: 150-5.
9. Abrams D, Brodie D and Arcasoy SM. Extracorporeal Life Support in Lung Transplantation. *Clinics in chest medicine*. 2017; 38: 655-66.
10. Martin JT and Zwischenberger JB. Artificial lung and novel devices for respiratory support. *Seminars in thoracic and cardiovascular surgery*. 2013; 25: 70-5.
11. Zwischenberger BA, Clemson LA and Zwischenberger JB. Artificial lung: progress and prototypes. *Expert review of medical devices*. 2006; 3: 485-97.

12. Zwischenberger JB, Anderson CM, Cook KE, Lick SD, Mockros LF and Bartlett RH. Development of an implantable artificial lung: challenges and progress. *ASAIO journal*. 2001; 47: 316-20.

13. Wu ZJ, Gellman B, Zhang T, Taskin ME, Dasse KA and Griffith BP. Computational Fluid Dynamics and Experimental Characterization of the Pediatric Pump-Lung. *Cardiovascular engineering and technology*. 2011; 2: 276-87.

14. Zhang JT, Nolan TDC, Zhang T, Griffith BP and Wu ZJJ. Characterization of membrane blood oxygenation devices using computational fluid dynamics. *J Membrane Sci*. 2007; 288: 268-79.

15. Schewe RE, Khanafer KM, Arab A, Mitchell JA, Skoog DJ and Cook KE. Design and in vitro assessment of an improved, low-resistance compliant thoracic artificial lung. *ASAIO journal*. 2012; 58: 583-9.

16. Madhani SP, Frankowski BJ, Ye SH, et al. In Vivo 5 Day Animal Studies of a Compact, Wearable Pumping Artificial Lung. *ASAIO journal*. 2019; 65: 94-100.

17. Orizondo RA, May AG, Madhani SP, et al. In Vitro Characterization of the Pittsburgh Pediatric Ambulatory Lung. *ASAIO journal*. 2018; 64: 806-11.

18. Madhani SP, Frankowski BJ, Burgreen GW, et al. In vitro and in vivo evaluation of a novel integrated wearable artificial lung. *The Journal of heart and lung transplantation : the official publication of the International Society for Heart Transplantation*. 2017; 36: 806-11.

19. Orizondo RA, Gino G, Sultzbach G, Madhani SP, Frankowski BJ and Federspiel WJ. Effects of Hollow Fiber Membrane Oscillation on an Artificial Lung. *Annals of biomedical engineering*. 2018; 46: 762-71.

20. D'Ancona G, Amaducci A, Rinaudo A, et al. Haemodynamic predictors of a penetrating atherosclerotic ulcer rupture using fluid-structure interaction analysis. *Interactive cardiovascular and thoracic surgery*. 2013; 17: 576-8.

21. Lee JJ, D'Ancona G, Amaducci A, Follis F, Pilato M and Pasta S. Role of computational modeling in thoracic aortic pathology: a review. *Journal of cardiac surgery*. 2014; 29: 653-62.

22. Pasta S, Gentile G, Raffa GM, et al. In Silico Shear and Intramural Stresses are Linked to Aortic Valve Morphology in Dilated Ascending Aorta. *European journal of vascular and endovascular surgery : the official journal of the European Society for Vascular Surgery*. 2017; 54: 254-63.

23. Pasta S, Phillippi JA, Tsamis A, et al. Constitutive modeling of ascending thoracic aortic aneurysms using microstructural parameters. *Medical engineering & physics*. 2016; 38: 121-30.

24. Rinaudo A and Pasta S. Regional variation of wall shear stress in ascending thoracic aortic aneurysms. *Proceedings of the Institution of Mechanical Engineers Part H, Journal of engineering in medicine*. 2014; 228: 627-38.

25. Catapano G, Papenfuss HD, Wodetzki A and Baurmeister U. Mass and momentum transport in extra-luminal flow (ELF) membrane devices for blood oxygenation. *J Membrane Sci*. 2001; 184(1): 123-5.

26. Svitek RG and Federspiel WJ. A mathematical model to predict CO2 removal in hollow fiber membrane oxygenators. *Annals of biomedical engineering*. 2008; 36: 992-1003.

27. Schlanstein PC, Limper A, Hesselmann F, Schmitz-Rode T, Steinseifer U and Arens J. Experimental method to determine anisotropic permeability of hollow fiber membrane bundles. *J Membrane Sci*. 2018; 546: 70-81.

28. Kaesler A, Rosen M, Schmitz-Rode T, Steinseifer U and Arens J. Computational Modeling of Oxygen Transfer in Artificial Lungs. *Artificial organs*. 2018; 42: 786-99.

29. International Organization for Standardization I. Cardiovascular implants and artificial organs — Blood-gas exchangers (oxygenators). 2016, p. 13.

30. Zhang T, Cheng G, Koert A, et al. Functional and biocompatibility performances of an integrated Maglev pump-oxygenator. *Artificial organs*. 2009; 33: 36-45.

31. Maquet Cardiohelp Technical Data Sheet:.

32. Fernando UP, Thompson AJ, Potkay J, et al. A Membrane Lung Design Based on Circular Blood Flow Paths. *ASAIO journal*. 2017; 63: 637-43.

33. Gartner MJ, Wilhelm CR, Gage KL, Fabrizio MC and Wagner WR. Modeling flow effects on thrombotic deposition in a membrane oxygenator. *Artificial organs*. 2000; 24: 29-36.

Figure legend

Figure 1: Cross section of the self-pumping oxygenation system showing the blood path and design of the rotating hollow-shaft with embedded fiber packages

Figure 2: Assembly of the self-pumping oxygenation system including 1) the rotating hollow-shaft, 2) PTFE rotary lip seals, 3) upper ball bearing and 4) lower ball bearing, 5) top housing and 6) bottom housing.

Figure 3: Sketch of the experimental setup for *in-vitro* gas exchange characterization of self-pumping artificial lung system

Figure 4: 3D streamlines in the self-pumping oxygenator device for the flow rate of 1 l/min and 2D cross-sectional (at the mid-line) view of the velocity field.

Figure 5: Fluid pressure distribution for the flow rate of 1 l/min and rotational speed of 1100 rpm

Figure 6: Distribution of shear stress in the self-pumping oxygenator device for the flow rate of 1 l/min and 2D cross-sectional (at the mid-line) view of the shear stress field.

Figure 7: (A) simulated oxygen saturation at flow rate of 1 l/min; overall oxygen transfer (B) and CO_2 removal (C) performance as determined by the numerical prediction (solid line) and experiments (dots) at different flow rate (standard deviation is based on two measurements); (D) *in-vitro* H–Q curve at different rotational speed using ovine blood at 37°C.

Table 1: Details of fiber packages and rotating shaft

	Self-Pumping Device
Fiber package angle	4 deg
Fiber package length and width	70 mm x 26 mm
Total fiber surface area	0.27 m^2
Shaft outer (inner) diameter	21 mm (12mm)
Shaft hole diameter	5 mm
Priming volume	110 ml
Gas inlet (outlet) port	6.35 mm (9.3 mm)
Blood inlet (outlet) port	9.5 mm (6.35 mm)

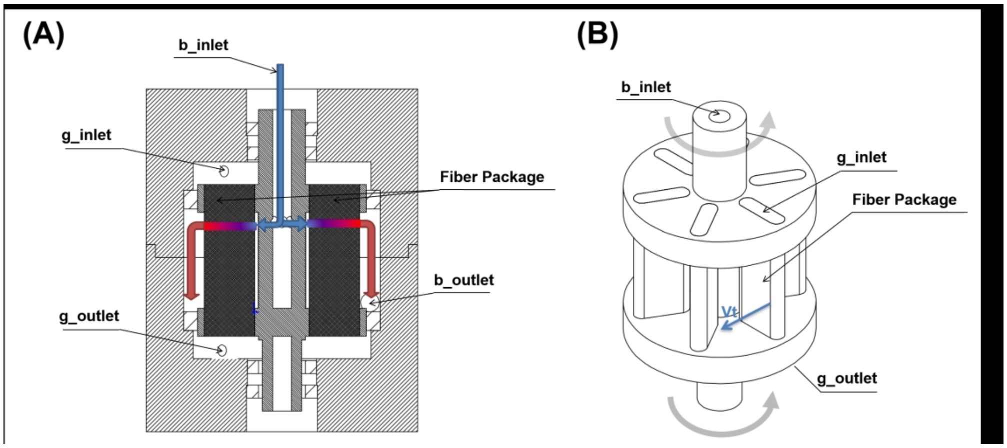

Figure 1

410x180mm (150 x 150 DPI)

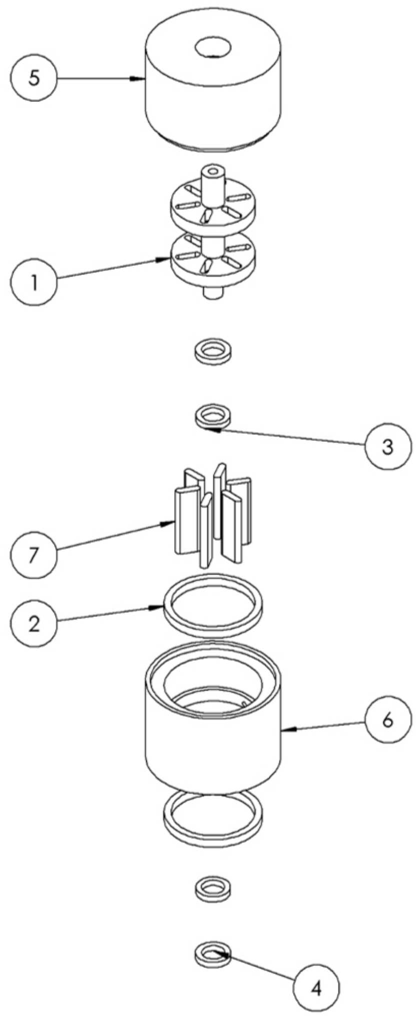

Figure 2

91x199mm (150 x 150 DPI)

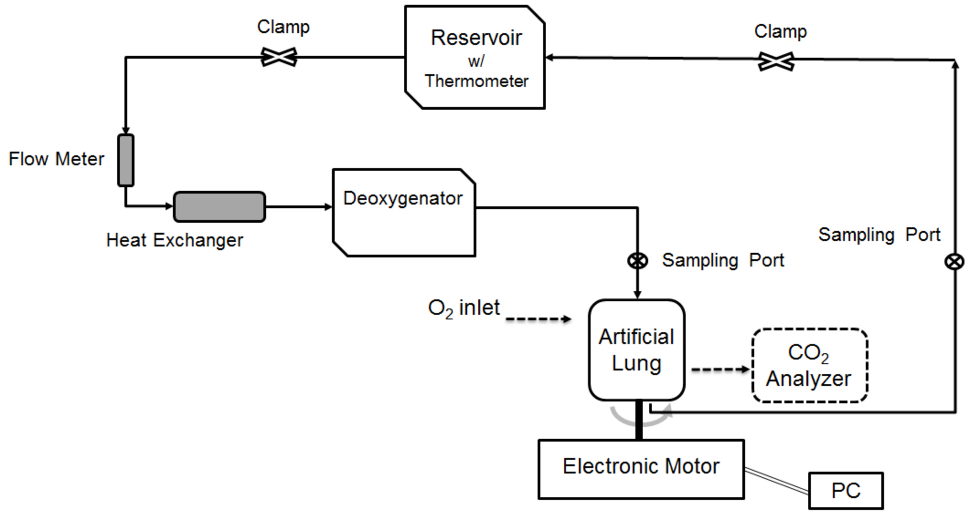

Figure 3

385x209mm (72 x 72 DPI)

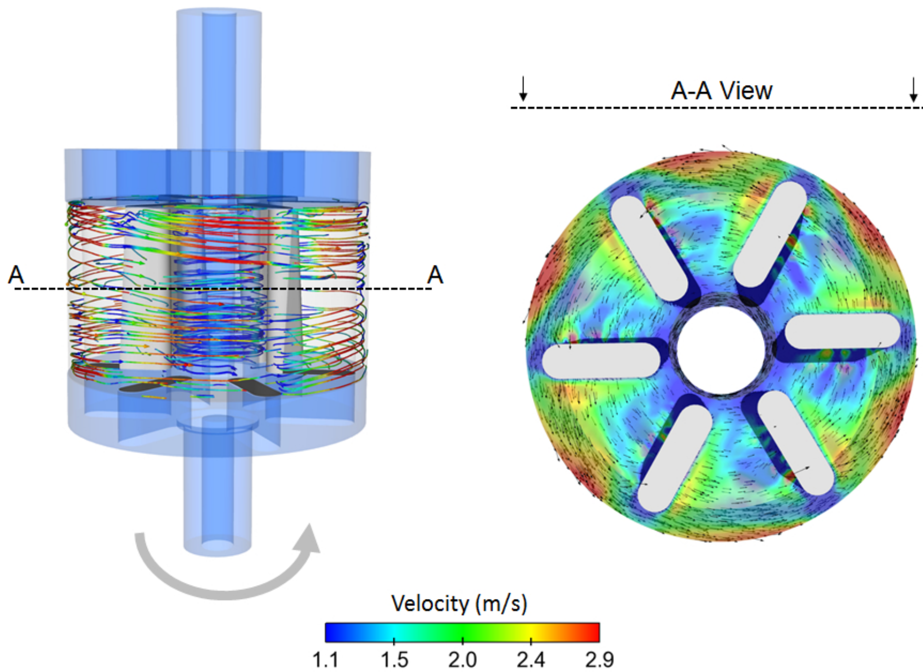

Figure 4

79x55mm (300 x 300 DPI)

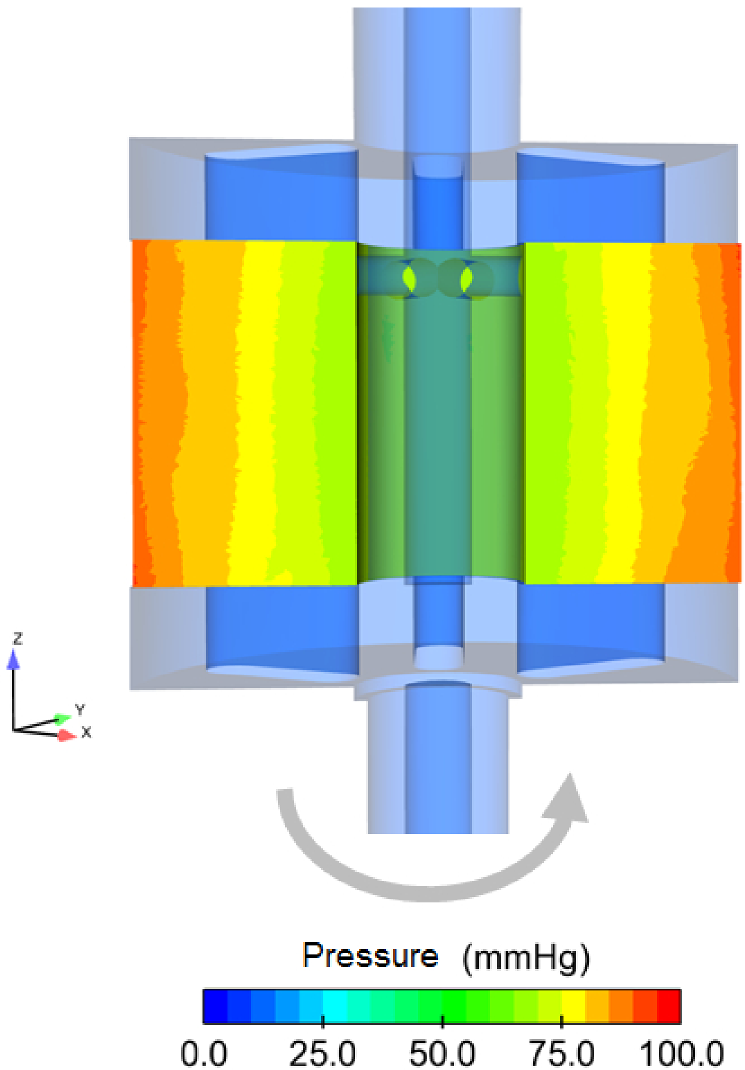

Figure 5

44x56mm (300 x 300 DPI)

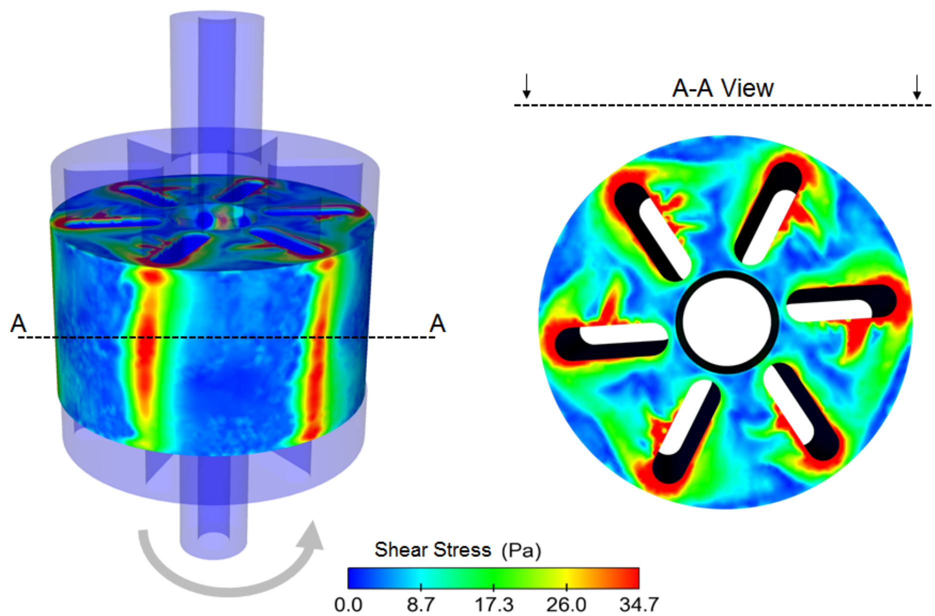

Figure 6

79x53mm (300 x 300 DPI)

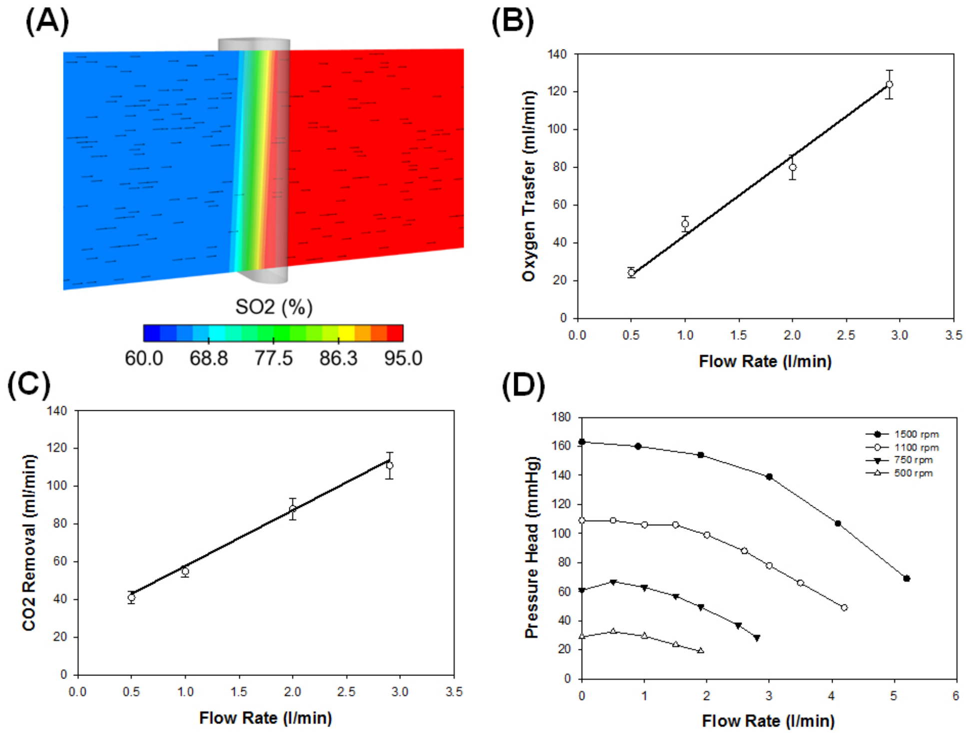

Figure 7

82x62mm (300 x 300 DPI)